Temporal integration of inductive cues on the way to gastrulation

Sarah McFann^{a,b}, Sayantan Dutta^{a,b}, Jared E. Toettcher^{c,1}, and Stanislav Y. Shvartsman^{b,c,d,1}

aDepartment of Chemical and Biological Engineering, Princeton University, Princeton, NJ 08544; bLewis Sigler Institute for Integrative Genomics, Princeton University, Princeton, NJ 08544; Department of Molecular Biology, Princeton University, Princeton, NJ 08544; and denter for Computational Biology, Flatiron Institute, Simons Foundation, New York, NY 10010

Edited by Norbert Perrimon, Harvard Medical School, Boston, MA, and approved April 20, 2021 (received for review February 9, 2021)

Markers for the endoderm and mesoderm germ layers are commonly expressed together in the early embryo, potentially reflecting cells' ability to explore potential fates before fully committing. It remains unclear when commitment to a single-germ layer is reached and how it is impacted by external signals. Here, we address this important question in Drosophila, a convenient model system in which mesodermal and endodermal fates are associated with distinct cellular movements during gastrulation. Systematically applying endoderminducing extracellular signal-regulated kinase (ERK) signals to the ventral medial embryo-which normally only receives a mesoderminducing cue-reveals a critical time window during which mesodermal cell movements and gene expression are suppressed by proendoderm signaling. We identify the ERK target gene huckebein (hkb) as the main cause of the ventral furrow suppression and use computational modeling to show that Hkb repression of the mesoderm-associated gene snail is sufficient to account for a broad range of transcriptional and morphogenetic effects. Our approach, pairing precise signaling perturbations with observation of transcriptional dynamics and cell movements, provides a general framework for dissecting the complexities of combinatorial tissue patterning.

germ layer specification | developmental signaling | transcriptional dynamics | morphogenesis | optogenetics

E ndoderm and mesoderm give rise to distinctly different tissues and structures, and yet, in a wide variety of triploblastic organisms, the specification of these germ layers is linked. Gastrulation of the endoderm and mesoderm occur synchronously in most species, with endodermal and mesodermal cells normally arising from progenitors that have already been spatially segregated from ectoderm precursors (1). Although each cell must eventually settle upon a single germ layer fate, coexpression of mesodermal and endodermal markers is common in cells before gastrulation (1, 2). In zebrafish, cells in the marginal zone express both gata5, an endodermal marker, and no tail (ntl), a mesodermal marker (3). In mice, the endodermal marker foxa2 and the mesodermal marker brachyury are both expressed in cells in the primitive streak (4). Coexpression tends to occur at early developmental time points and ceases over time, with cells that once coexpressed both sets of markers commonly adopting endodermal fates. In some cases, however, cells exhibit bipotential, as in the zebrafish embryo in which a subset of cells in the marginal zone produces both endodermal and mesodermal daughter cells (5, 6). In all organismal contexts, the levels of endodermal and mesodermal markers change over time. Here, we investigate how and when cells interpret these cues to make critical decisions about cell fate and gastrulation.

One of the best-studied examples of mesodermal/endodermal coexpression occurs in the early Drosophila embryo. Mesoderm is formed along the ventral surface of the embryo in response to Dorsal (DI) signaling downstream of Toll activation, whereas endoderm is formed at the embryo poles in response to extracellular signal-regulated kinase (ERK) signaling downstream of Torso activation. While ERK plays additional roles in the pregastrulation embryo, such as acting with DI to pattern neural ectoderm in the ventrolateral embryo (7-9), it is primarily proendodermal when

activated early and for long duration (10-12). Global hyperactivation of ERK induces proendoderm genes like tailless (tll) and huckebein (hkb) throughout the embryo and represses the genes needed for specifying future mesoderm and neural ectoderm. In wild-type embryos, ERK is activated early and in a prolonged manner at ventral posterior positions where Torso and Toll signals overlap, exerting a proendodermal effect by inducing genes like tll and hkb, even as Dl exerts a promesodermal influence by inducing genes like twist (twi) and snail (sna) (13).

In the Drosophila embryo, mesoderm-fated cells undergo pronounced, stereotyped cell movements early during gastrulation as they invaginate to form the ventral furrow. In wild-type embryos, the ventral furrow does not extend to the posterior and anterior poles, where Hkb represses sna (14-16). Prior studies hint at complex interplay between endoderm- and mesoderm-inducing signals at the poles: ERK signaling represses sna more efficiently at the posterior pole than at the anterior pole (17), leading to stronger ventral furrow suppression at the posterior (15, 18). The ventral furrow decision is an excellent model system for studying the integration of endodermal and mesodermal cues for several reasons: with live imaging, it is easy to identify the mesoderm cells participating in ventral furrow formation, and with optogenetic tools already developed for Drosophila (19, 20), ERK signaling can be applied to any embryonic region at will. By applying ERK signaling to the ventral medial region of the embryo, which normally only receives DI signaling, we can study how cells interpret two concurrent inductive signals to make a ventral furrow decision.

Another question is how cells integrate information coming in from ERK and DI signaling. In addition to the Hkb-dependent repression of sna, ERK signaling antagonizes Dl signaling through the

Significance

In early development, cells commit to a single germ fate despite receiving multiple, conflicting inductive cues. Here, we examine how cells in the Drosophila embryo integrate promesodermal and proendodermal signals. We find that proendoderm signals repress transcriptional determinants of mesodermal cell movements during a critical time window in the early embryo. Based on precise optogenetic perturbations, live imaging, and computational modeling, our work provides a framework for quantitative understanding of combinatorial control of gastrulation

Author contributions: S.M., J.E.T., and S.Y.S. designed research; S.M. and S.D. performed research; S.D. contributed new reagents/analytic tools; S.M. analyzed data; and S.M., S.D., J.E.T., and S.Y.S. wrote the paper.

The authors declare no competing interest.

This article is a PNAS Direct Submission.

Published under the PNAS license

¹To whom correspondence may be addressed. Email: toettcher@princeton.edu or stas@ princeton.edu.

This article contains supporting information online at https://www.pnas.org/lookup/suppl/ doi:10.1073/pnas.2102691118/-/DCSupplemental.

Published June 3, 2021.

expression of *wntD*, a gene that is induced by both ERK and DI and encodes a secreted protein that interferes with Toll receptor activation (21–24). *wntD* is further regulated by DI's downstream targets *twi* and *sna* (24). Overexpression of *wntD* has been shown to repress *sna* and suppress ventral furrow formation, making the WntD pathway a second arm through which ERK signaling can inform the ventral furrow decision (24). It is unclear how the *hkb* and *wntD* repressive arms act in tandem and how much each arm contributes to the down-regulation of *sna* expression and ventral furrow suppression.

We set out to quantitatively address these questions by applying precise doses and durations of endoderm-inducing ERK signaling to the ventral medial region of the embryo. By observing the resulting *sna* transcription and morphogenetic movements, we find that only a brief pulse of ERK signaling is required to prevent ventral furrow formation. We further find that the embryo is not equally sensitive to ERK signaling over time—ventral furrow formation is only inhibited when ERK signaling is applied during a specific time window spanning the 13th and 14th nuclear cycles

(NC13 and NC14). We trace the consequences of ERK activation to downstream gene expression, revealing that NC14 *sna* transcription is attenuated, and show that ERK activation prior to the critical window leads to changes in *sna* timing, an effect that is tightly correlated with the timing of ventral furrow invagination. Through additional genetic perturbations, we find that Hkb rather than WntD is primarily responsible for attenuation of *sna* expression. Finally, we show via computational modeling that Hkb repression of *sna* is sufficient to explain our data, including dynamic features of *sna* transcription, the timing of the critical ERK signaling window, and ventral furrow timing. Taken together, our results indicate that endodermal and mesodermal cues are integrated in the *Drosophila* embryo during a narrow temporal window at the level of *sna* to dictate the position and timing of ventral furrow formation.

Results

Optogenetic ERK Signaling Prevents Ventral Furrow Formation. We focused on the ventral medial region of the embryo, which receives

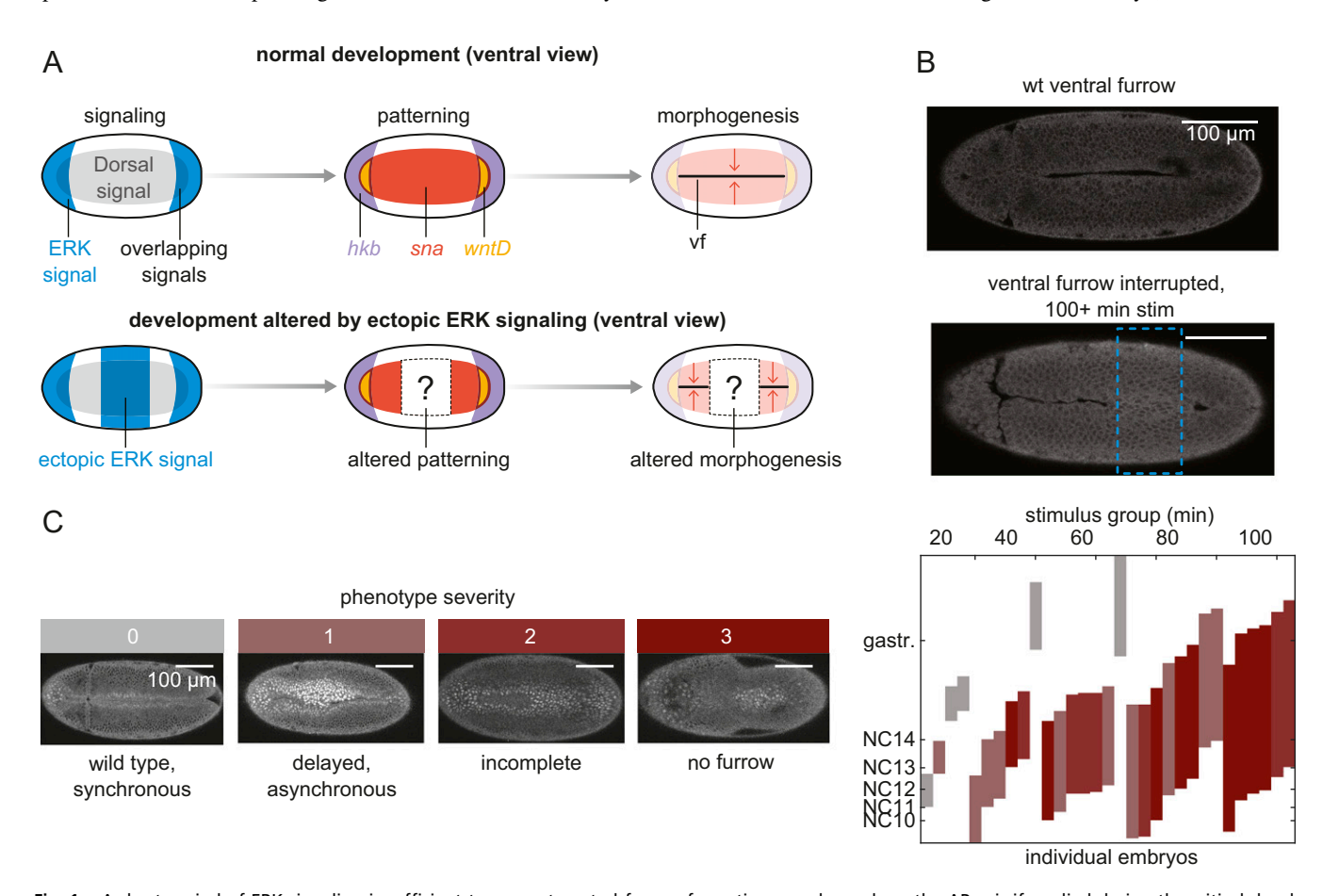


Fig. 1. A short period of ERK signaling is sufficient to prevent ventral furrow formation anywhere along the AP axis if applied during the critical developmental window. (A) Schematic of the ventral embryo describing signaling, patterning, and morphogenesis relevant to the ventral furrow decision (top row). DI signaling (gray) occurs ventrally and overlaps ERK signaling (blue) at the embryo termini. Signaling patterns transcription: sna transcription (orange) occurs downstream of DI signaling while hkb transcription (purple) occurs downstream of ERK signaling. Where DI and ERK signaling overlap, wntD (yellow) is transcribed. Sna initiates cellular movements (orange arrows) that result in ventral furrow (black line) formation. The ventral furrow does not extend to the embryo termini due to repression from Hkb and WntD. In experiments (bottom row), we apply ectopic ERK signaling of various durations to the center of the embryo, as shown by the blue rectangle of ectopic ERK signal in the bottom figure, and we observe how patterning and ventral furrow formation are altered. (B) Image of an unstimulated embryo and an embryo stimulated for 100+ min in an 80 μm stripe applied to the embryo center, as indicated by the dotted blue box. Light stimulation interrupted ventral furrow formation locally. The marker shown is OptoSOS-tRFP. (C) Ventral furrow phenotypes observed downstream of light stimulus conditions. The marker shown is DI-Venus. Blue light was applied to the entire field of view shown. Severity 0 indicates wild-type (synchronous) ventral furrow formation. Severity 1 indicates delayed and asynchronous furrow formation, as shown by the in-progress ventral furrow that has invaginated on the right and left regions of the embryo but not the center. Severity 2 indicates incomplete furrow invagination, as shown by the furrow only on the left embryo. Severity 3 indicates no furrow. In the plot on the right, each vertical bar represents an embryo and the times over which the embryo received stimulation. Phenotype sev

high levels of nuclear Dl but no ERK signaling (Fig. 1A). Previous work has shown that overexpression of *hkb* is sufficient to completely block ventral furrow invagination (18), analogous to the ventral furrow suppression that occurs natively at the embryo poles downstream of *hkb*. This suggests that cells in the medial embryo are indeed sensitive to ERK signaling, even if they do not experience it in a wild-type embryo, and that these cells' responses can be used to explore the developmentally relevant process of ventral furrow suppression. We sought to determine whether—and at which developmental times—an optogenetic ERK signal is sufficient to block ventral furrow formation in otherwise ERK-naïve cells.

We generated an ectopic ERK signal using OptoSOS, an optogenetic system that induces ERK signaling by translocating the protein SOS to the plasma membrane (19, 25). We illuminated OptoSOS embryos using 450 nm light delivered to the center of the embryo. The light penetrated each embryo fully in the z-direction but confined gene expression downstream of ERK to within 5 to 10 μ m of the stripe in the x- and y-direction (SI Appendix, Fig. S1). Illumination was delivered in 100-msec pulses every 20 s, leading to ERK activity comparable to our prior work (Materials and Methods) (26). We found that illumination from NC10 through NC14 was sufficient to disrupt ventral furrow in the region where light was applied (Fig. 1B), and global illumination from NC10 to NC14 blocked ventral furrow across the entire ventral medial region (Movie S1). Thus, ectopic ERK signaling applied to the ventral medial embryo suppresses the effects of Dl in a manner analogous to what occurs natively in the ventral posterior or in the ventral medial region of hkb-overexpressing embryos.

NC13 and Early NC14 Constitute a Critical Window for Signal Integration.

Having determined that long-lasting ERK signaling is sufficient to interrupt ventral furrow formation, we set out to determine the minimal duration of light sufficient for this effect. Stimuli consisted of 20, 40, 60, 80, or 100 min of blue light initiated sometime between the beginning of NC10 and the end of NC14, and each stimulus was applied across the ventral medial region of an embryo containing OptoSOS and a Dl-Venus reporter construct (27). Phenotypes were scored between 0 and 3 based on how severely the ventral furrow was affected (Fig. 1C). We assigned a score of 0 for ventral furrows that were indistinguishable from wild-type embryos. At the other extreme, embryos in which no ventral furrow formed received a score of 3. A score of 2 denoted embryos that only formed a portion of the normal ventral furrow. Finally, a score of 1 denoted embryos in which ventral furrow formation was delayed and asynchronous but complete (i.e., the entire region that would have invaginated in a wild-type embryo did invaginate). We observed delays ranging from 15 min to 1 h.

As expected, longer durations of blue light caused more severe phenotypes (*SI Appendix*, Fig. S24). While 20 min of stimulus was insufficient to completely eliminate the ventral furrow, 40 min was sufficient but only when applied beginning in NC13. In general, stimuli of all durations were more effective at suppressing ventral furrow formation when applied across NC13 and early NC14 than stimuli applied NC10 through NC12 or stimuli applied mid-NC14 through late-NC14 (*SI Appendix*, Fig. S2*B*). The heightened susceptibility observed during NC13 and early NC14 is notable given that native ERK signaling is sustained at the termini over a much longer period, from NC10 until gastrulation (28, 29). Our data thus indicate that there is a critical window during which ERK signaling exerts a suppressive effect on ventral furrow patterning.

ERK Signaling Alters the Level and Dynamics of sna Transcription.

Seeing that ERK signaling duration affects the severity of gastrulation phenotypes, we hypothesized that these differences could be explained at the level of *sna*, a master regulator of ventral furrow morphogenesis that is negatively regulated by ERK (14–16, 24, 30). We applied an identical protocol of 450 nm light to embryos

containing OptoSOS, MCP protein, and a BAC transgene reporter containing the complete regulatory region upstream of *sna*, which served as a proxy for visualizing *sna* transcription (31). In wild-type embryos, the total amount of *sna* transcription approximately doubled each nuclear cycle, reflecting the doubling number of transcribing nuclei, but in embryos that received blue light from NC10 through NC14, *sna* was drastically attenuated and expressed at a low level throughout all nuclear cycles (Fig. 24). Studies with fixed wild-type embryos previously established that sustained ERK signaling down-regulates *sna* at the posterior pole (14–16, 24). Consistent with these studies, we found that delivering sustained ERK activity to the ventral medial region of the embryo markedly decreases *sna* MS2 activity.

Having observed that short durations of ERK signaling can suppress the ventral furrow (Fig. 1C), we next investigated how similar ERK stimuli alter sna dynamics. A 60-min light stimulus was applied over three different periods: NC10 through NC13, NC12 through early NC14, and NC14 (Fig. 2B). The NC12 through early NC14 period overlapped the previously identified critical window, so we termed the NC10 through NC13 stimulation period as "early" relative to the critical window and NC14 stimulation as "late." All three stimulation conditions led to reduced sna transcription in NC14. However, stimulation across the critical window led to almost complete loss of NC14 sna transcription (Fig. 2 B, Right), while early and late stimulation resulted in only modest reduction. While peak NC14 sna transcription occurred at the same time for late stimulation as for wild-type embryos (Fig. 2 B, Left), peak transcription was delayed by ~15 min in embryos stimulated early (Fig. 2 B, Middle). Taken together, our data demonstrate that changing the timing of ERK signaling results in different dynamic profiles of sna, with signaling during the critical window resulting in the most dramatic attenuation.

The Level and Timing of sna Transcription Predicts Ventral Furrow Position and Timing. Varying the time and duration of ERK signaling resulted in morphogenetic phenotypes that ranged in severity (Fig. 1C). As different ERK signaling periods and durations also result in different sna dynamics (Fig. 2 A and B), we hypothesized that sna dynamics and ventral furrow phenotypes are correlated. Such a link would be supported by prior studies. Ventral furrow formation is thought to require Sna-dependent expression of the G protein coupled receptor (GPCR) Mist, which is activated by Fog, a GPCR ligand expressed downstream of Dl signaling and the transcription factor Twi (32–34). Mist activation induces Rho signaling that results in the activation of Myosin II on the apical surfaces of cells (35–39), which is responsible for ventral furrow formation (40, 41).

To test whether the amount of *sna* transcription is predictive of the extent of ventral furrow invagination, we plotted the percentage of the illuminated region that invaginated versus the number of sna-transcribing nuclei in NC14 for 15 individual embryos (Fig. 2C). We found that ventral furrow length was similar for wild-type embryos and embryos exposed to either early or late ERK stimuli. All embryos in these groups possessed at least 35 active nuclei, though some unstimulated embryos had as many as 220 active nuclei. In contrast, embryos stimulated across the critical window or continuously from NC10 through NC14 showed severe reductions in ventral furrow formation, and all these embryos had fewer than 35 active nuclei. Our data suggest that sna expression above a threshold is required to trigger ventral furrow formation. While wild-type embryos substantially exceed this threshold, stimulation during the critical window drops sna expression to levels that no longer support mesoderm invagination.

Although *sna* transcription in the nuclear cycles preceding NC14 differs only subtly among our stimulation conditions, when we included *sna* transcription from NC10 through NC13 in our invagination analysis, we found we were better able to differentiate between continuously illuminated embryos and embryos that

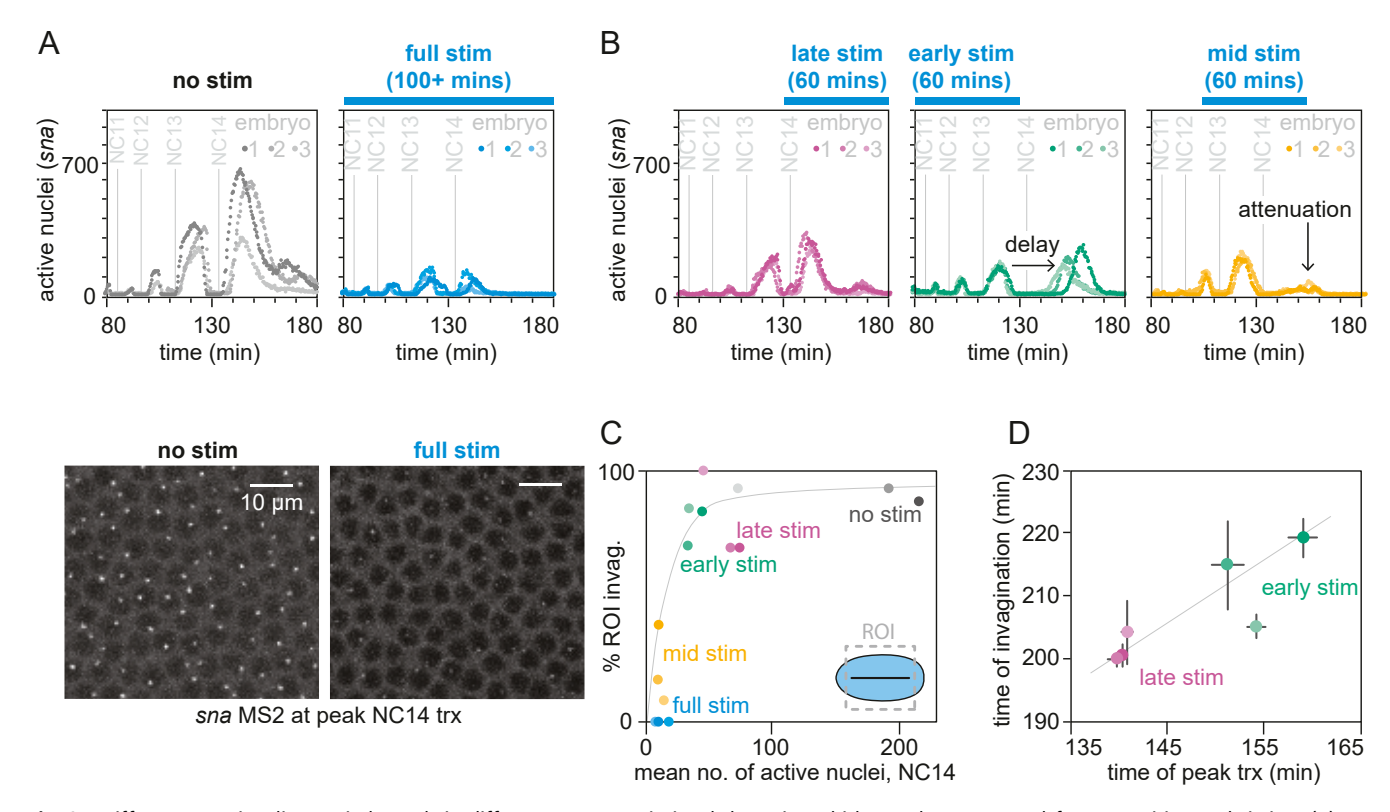


Fig. 2. Different ERK signaling periods result in different sna transcriptional dynamics, which correlate to ventral furrow position and timing. (A) sna transcriptional dynamics in the presence (blue, n=3) and absence (gray, n=3) of "full stimulation" (i.e., 100+ minutes of ERK signaling) using a sna BAC > MS2 transgene reporter. The x-axis represents developmental time, and the y-axis represents the number of nuclei transcribing sna in the ROI (Fig. 2C). The blue bar represents the full-stimulation light time course. Representative images of transcribing cells were taken at the time of peak NC14 sna transcription from the center of the embryo where ectopic ERK signaling was applied. (B) sna transcriptional dynamics from embryos stimulated with blue light in order of increasing phenotype severity: stimulated for 60 min beginning in the mitosis prior to NC14 (late, pink), stimulated for roughly 60 min NC10 through NC13 (early, green), and stimulated for 60 min beginning in the mitosis prior to NC12 (middle—i.e., applied across the critical window, yellow). The blue bar above each plot represents the time course of light stimulation. The x-axis represents developmental time, and the y-axis represents the number of nuclei transcribing sna in the ROI (C). n=3 per stimulus condition. Early stimulation leads to delayed NC14 sna transcription, and "middle" stimulation leads to attenuated NC14 sna transcription. (C) Percent of ROI that invaginates versus the mean number of sna transcribing nuclei in NC14. The embryos are the same as those shown in A and B (n=15). The black dotted rectangle imposed over the cartoon of a light-stimulated embryo shows the field of view/ROI, and the black line indicates the ventral furrow. The gray curve highlights that when the mean number of active nuclei is above 35, the percent of the ROI that invaginates is roughly constant. (D) Time of ventral furrow invagination versus time of peak NC14 sna transcription. "Early stim" (green) and "late stim" (p

received stimulation only during the critical window (*SI Appendix*, Fig. S3). Embryos stimulated from NC10 through NC14 possess 10 to 20 active nuclei, while embryos stimulated across the critical window possess 25 to 30 active nuclei. Thus, it appears that *sna* activity in NC10 through NC13 can become important for determining ventral furrow formation when *sna* activity in NC14 is low or absent, leading to differences between continuous and critical-window stimulation.

To further refine our picture of how *sna* expression relates to morphogenesis, we sought to compare the relative timing of *sna* transcription to the timing of invagination. For this analysis, we focused on early- or late-stimulated embryos: both classes invaginated completely (Fig. 2C) and exhibited similar levels of *sna* transcription (Fig. 2B and *SI Appendix*, Fig. S3). However, peak NC14 *sna* transcription occurred ~15 min later in early-stimulated embryos compared to those stimulated late. Indeed, plotting the time of ventral furrow invagination against the time of peak NC14 *sna* transcription revealed that the two variables were tightly correlated (Fig. 2D). Late-stimulated embryos invaginated at a time comparable to wild-type embryos, but invagination in early-stimulated embryos was delayed ~15 min, matching their delay in NC14 *sna* expression. This result

suggests that the timing of invagination is dictated by the timing of NC14 sna expression.

Together, these results show that *sna* transcriptional dynamics dictate the timing of ventral furrow invagination, in addition to determining whether invagination occurs at all. Complete invagination only occurs when the number of active nuclei in NC14 exceeds a threshold value (Fig. 2C), and in embryos with sufficiently high levels of NC14 *sna* expression, the timing of peak expression predicts the time of invagination (Fig. 2D). Combined with the results of Fig. 1C, a clearer picture of endodermal/mesodermal signal integration in the early *Drosophila* embryo begins to emerge: through repressive action, ERK signaling dynamics drive a dynamic pattern of *sna* transcription, which then dictates if and when the ventral furrow forms.

ERK Signaling Represses *sna* **via Hkb and the** *sna* **Distal Enhancer.** We have seen that ERK activity attenuates and delays *sna* expression, but how is this repressive influence achieved? ERK signaling is thought to repress *sna* transcription in several ways: ERK drives *hkb* expression, which represses *sna* expression (14–16), and ERK triggers *wntD* expression that is thought to inhibit the Toll receptor and attenuate Dl-mediated *sna* activation (Fig. 3*A*) (21–24). We sought to understand how each mechanism contributes to the

regulation of *sna*. We first generated embryos containing Opto-SOS, MCP-mCherry, and MS2 reporters for either *hkb* or *wntD* (26, 42) to measure ERK-induced expression of the two genes. Both *hkb* and *wntD* transcription were rapidly and potently initiated by light-induced ERK activity as early as NC10 (Fig. 3 B and C), indicating that either repressive arm could be responsible for the ERK-dependent alteration of *sna* transcription in NC14.

We set out to decouple the effects of Hkb and WntD on sna transcription using reporters for specific portions of the sna enhancer region. To this end, we employed a reporter for the sna distal enhancer (sna DE) that contains both Dl- and Hkb-binding sites and a reporter for the sna proximal enhancer (sna PE) that lacks Hkb-binding sites (Fig. 3A) (23). We reasoned that by comparing light-triggered responses between the sna PE, sna DE, and full-length reporters, we might separate Hkb-dependent from Hkbindependent repression of sna. Indeed, we observed that the Hkbsensitive sna DE showed attenuation in response to light-induced ERK activation during NC14 (Fig. 3D), as was observed for the full-length sna reporter with both enhancers (Fig. 24). In contrast, the activity of the sna PE reporter showed no difference in NC14 expression levels between light-stimulated and unstimulated regions of the embryo (Fig. 3D). As only the sna DE reporter showed decreased NC14 activity in response to long-lasting ERK signaling, we conclude that the distal enhancer is predominantly responsible for sna repression by ERK signaling, likely via Hkb.

As an independent method to confirm that WntD does not play a major role in ERK-mediated ventral furrow suppression,

we repeated the experiment of Fig. 1*C* in OptoSOS embryos lacking Fz4, the maternally-deposited receptor through which WntD inhibits Dl signaling (*SI Appendix*, Fig. S4) (43). We saw no distinguishable differences in phenotypic severity between light-stimulated *fz4* and wild-type OptoSOS embryos, indicating that WntD is dispensable for both the overall effect and the dynamics with which ERK suppresses ventral furrow formation.

A Computational Model Recapitulates ERK Suppression of the Ventral Furrow. Our experiments indicate a complex relationship between the timing of ERK activation and the dynamics of *sna* transcription. Early and late stimulation modestly attenuate NC14 *sna* transcription, stimulation across the critical window greatly attenuates NC14 *sna* transcription, and early stimulation delays NC14 *sna* transcription. Additionally, all these dynamics play out in the context of an embryo with changing levels of key transcription factors like Dl (27) and in which rapid nuclear division cycles repeatedly double the number of potential sites of transcription. To gain further insight into how complex spatial and temporal patterns of signaling and transcription are related, we established a computational model of both processes.

Our computational approach is based on a model we described recently that takes into account the three-dimensional nature of the embryo, nuclear doubling, and the positions of nuclei at each nuclear cycle (44, 45). We focused on a $\sim 400 \times 200 \ \mu m$ region around the ventral-most point of the embryo to represent the region illuminated in our experiments (*SI Appendix*, Fig. S5B). ERK

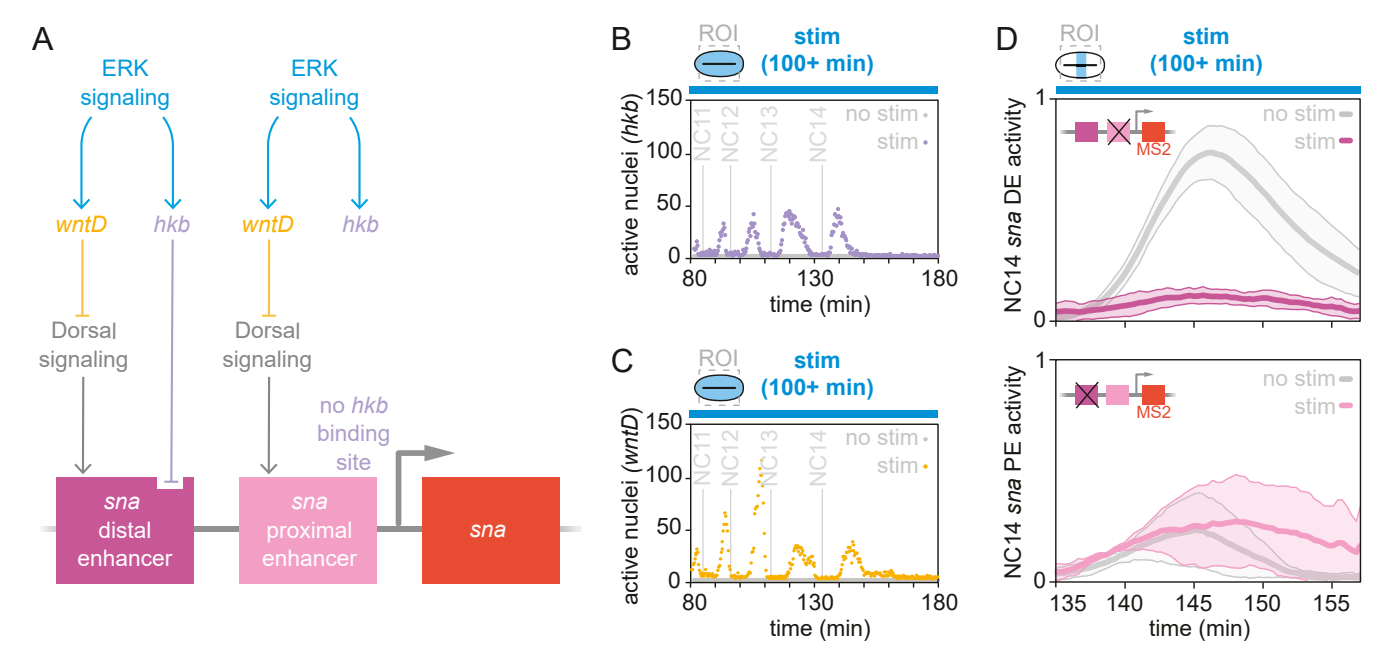


Fig. 3. Hkb repression alone is sufficient to explain sna transcriptional dynamics downstream of ERK signaling. (A) Diagram depicting how ERK signaling differentially regulates sna's two enhancers. DI induces sna transcription, and ERK induces hkb and wntD transcription. Hkb represses sna at the DNA level while WntD down-regulates DI signaling. Hkb only acts on the distal enhancer. (B) hkb transcriptional dynamics in OptoSOS embryos in the presence of 100+ min of blue light stimulation. The x-axis represents developmental time, and the y-axis represents the number of nuclei transcribing hkb in the region of interest, depicted by the dashed gray box. The purple trace is from a stimulated embryo while the gray trace is from an unstimulated embryo (n = 2, 1 per condition). A cartoon embryo is included to show the ROI, and that light was applied globally. (C) wntD transcriptional dynamics in OptoSOS embryos in the presence of 100+ min of blue light stimulation. The x-axis represents developmental time, and the y-axis represents the number of nuclei transcribing wntD in the region of interest, depicted by the dashed gray box. The yellow trace is from a stimulated embryo while the gray trace is from an unstimulated embryo (n = 2, 1 per condition). A cartoon embryo is included to show the ROI, and that light was applied globally. (D) Light stimulation does not affect NC14 expression from the sna proximal enhancer but attenuates expression from the distal enhancer. A cartoon embryo is included at the top of the plot to show that a thick stripe of light was applied down the center of embryos, leaving the left and right sides of embryos unstimulated. A dashed gray box shows the region from which images were collected. The y-axes of the plots show enhancer activity, and the x-axes show developmental time. In the top plot, the solid gray line shows the activity of the sna distal enhancer in NC14 in the unstimulated embryo region, while the solid magenta line shows enhancer activity in the stimulated region. Shaded regions indicate the SD (n = 3). A cartoon shows that the MS2 reporter only contains the distal enhancer. In the bottom plot, the solid gray line shows the activity of the sna proximal enhancer in NC14 in the unstimulated region, while the solid pink line shows enhancer activity in the stimulated region. Shaded regions indicate the SD (n = 3). A cartoon shows that the MS2 reporter only contains the proximal enhancer.

and Dl signaling were modeled as spatially distinct reaction-diffusion equations over the surface of the embryo. Transcription of *hkb* and *sna* were represented as stochastic events governed by protein concentrations. When the amount of ERK protein is high, *hkb* transcription is likely. When the amount of Dl protein is high and Hkb protein is low, *sna* transcription is likely. Since *sna* expression natively attenuates toward the end of NC14 even in the absence of ERK signaling, a parameter in our model sets a cutoff time after which *sna* becomes highly improbable to transcribe.

We estimated the parameters of the model to qualitatively match the *sna* transcriptional dynamics in Fig. 2 A and B. The corresponding model trajectories are shown in *SI Appendix*, Fig. S6 and reproduce the NC14 delay in peak *sna* transcription in early-stimulated embryos and the large attenuation triggered by stimulation during the critical window. We next simulated our model under the full set of stimulation conditions shown in Fig. 1C. We employed Sna protein integrated over time as a proxy for phenotype. According to data shown in *SI Appendix*, Fig. S3, embryos are able to initiate ventral furrows when the mean number of *sna*-active nuclei exceeds ~20, and embryos exhibit a wild-type phenotype when the mean number of active nuclei exceeds ~50. We used our model to convert these threshold values into integrated Sna protein values (*SI Appendix*, Fig. S7), which we then used to predict the phenotypic severity (Fig. 4A).

Our model recapitulated the existence of a critical signaling window. For short ERK inputs, stimulation in NC13 and early NC14 caused the largest reduction in integrated Sna protein (Fig. 4A). To better understand this critical window, we examined the predicted dynamics of Sna and Hkb protein levels over time in embryos of varying phenotypic severity (SI Appendix, Fig. S8). As expected in light of our data (Fig. 24), Sna protein levels peaked strongly in early NC14 in wild-type embryos, while embryos with the most severe phenotypes exhibited low Sna in early NC14 (SI Appendix, Fig. S8, upper row). The Hkb trajectories did not exhibit so obvious a trend: late-stimulated embryos that exhibited a wild-type phenotype reached the same high levels of Hkb in late NC14 as did embryos exhibiting the most severe phenotype, while early-stimulated embryos exhibiting moderately severe phenotypes accumulated less Hkb overall (SI Appendix, Fig. S8, lower row). Though the overall Hkb trajectories did not correlate with phenotypic severity, Hkb levels in the first ~7 min of NC14 did correlate with severity: embryos with high Hkb levels in early NC14 exhibited severe phenotypes, while embryos with low levels during this period presented as wild type (SI Appendix, Fig. S8, lower row). This result suggests that because NC14 produces the most sna, the most effective ERK signaling interventions generate high levels of Hkb in time to repress sna in early NC14.

A sensitivity analysis of the model demonstrated that the critical time window was best controlled by parameters that affected the persistence of ERK-induced Hkb expression or the strength of Hkb-mediated *sna* repression (*SI Appendix*, Table S2). For example, decreasing Hkb's degradation rate increased its ability to repress *sna*, widening the critical window to earlier signaling periods (*SI Appendix*, Fig. S9). No parameter could extend just the late boundary of the critical window, since our model holds that the cumulative dose of Sna protein is what determines the level of ventral furrow suppression, and it is thus too late to suppress Sna effectively once it has already been produced.

We then asked whether the model could predict ventral furrow delays. Using the integrated Sna threshold value that corresponds to ~20 active nuclei (SI Appendix, Fig. S7), the number of active nuclei presumably required for an embryo to initiate invagination (SI Appendix, Fig. S3), we used our model to see whether the time at which Sna protein exceeded the threshold changed depending on the stimulation condition (Fig. 4B). In unstimulated embryos and embryos stimulated late, the threshold was exceeded almost as soon as NC14 began. In embryos stimulated early, the threshold was exceeded ~15 min later than

in late-stimulated embryos, just as we observed experimentally (Fig. 2D). These virtual embryos also exhibited a \sim 20 min delay in NC14 peak sna transcription, similar to early-stimulated embryos in our experiments (Fig. 2D). Thus, our model recapitulates our experimental observation that delays in peak sna transcription correspond to delays in ventral furrow invagination.

Taken together, our model demonstrates that nuclear cycle doubling, natural attenuation of *sna* transcription in late NC14, and the timing of Hkb accumulation are sufficient to explain our experimental observations. A single model output—the integrated amount of Sna protein—not only predicts the presence or absence of a ventral furrow but also how the timing of ventral furrow invagination is altered by different dynamics of mesoderm-suppressing ERK signaling.

Discussion

We identified a critical time window during which ERK signaling is able to suppress mesoderm-associated formation of the ventral furrow. Computational modeling, imaging, and genetic perturbations revealed that ERK's inhibition of ventral furrow invagination can be quantitatively explained by a simple genetic circuit: ERK triggers hkb expression, leading to repression of the mesoderm-associated gene sna. A simple threshold in sna transcription is sufficient to predict whether embryos produce a ventral furrow, and the timing of NC14 sna expression predicts when ventral furrow invagination will occur (Fig. 4C). This simplicity was unexpected, given the complexity of the genetic circuits that have been implicated in ventral furrow formation, involving multiple negative regulators (hkb and wntD) and multiple furrow-inducing genes (sna and twi).

In addition to specifying endodermal cell fates, ERK signaling patterns the tail, the head, the eighth abdominal segment, and the cell movements underlying posterior midgut invagination (10, 46). How does the dose of ERK signaling required to suppress mesoderm cell movements compare to that required to activate these diverse endoderm-related processes? In prior work, we determined that posterior patterning was rescued by progressively increasing ERK doses in a particular order: forming tail structures requires the shortest duration of ERK signaling, followed by the eighth abdominal segment and then endodermal cell movements, which require the longest duration (26). When applied globally, long-duration ERK signaling triggered endoderm-associated gene expression and apical constriction across the whole embryo. Here, we find that mesodermal cell movements can be blocked by a much shorter duration of ERK signaling (~40 min under this study's illumination conditions) than that required to induce such a whole embryo "squeeze" (~100 min) (Fig. 1C and Movie S2). Because endogenous ERK signaling is delivered in a gradient at the anterior and posterior poles, it is possible that this difference in sensitivity enables the embryo to spatially separate two different morphogenesis events: mesodermal invagination of the ventral furrow and endodermal invagination of the posterior midgut.

Our work also provides context for studies that describe cell-cell communication and mechanochemical feedback along the ventral furrow. It was recently shown that the sna-dependent accumulation of Myosin II foci in some cells is sufficient to induce mesoderm invagination in neighboring cells through a Fog-dependent mechanism (47). We find, however, that ventral furrow can be locally suppressed by optogenetic ERK stimulation, even in the presence of sna-dependent furrow formation on either side of the illuminated region (Fig. 1B). These data indicate that ERK signaling suppresses not only a cell's intrinsic commitment to furrow formation but also blocks inductive furrow formation from neighboring cells, possibly through ERK-dependent induction of fog and mist (12) that disrupt signal propagation from DI-dependent fog expression. In future studies, it would thus be interesting to examine molecular events associated with invagination (e.g., fog and mist expression; Myosin II localization) in cells receiving both proendoderm and promesoderm signaling.

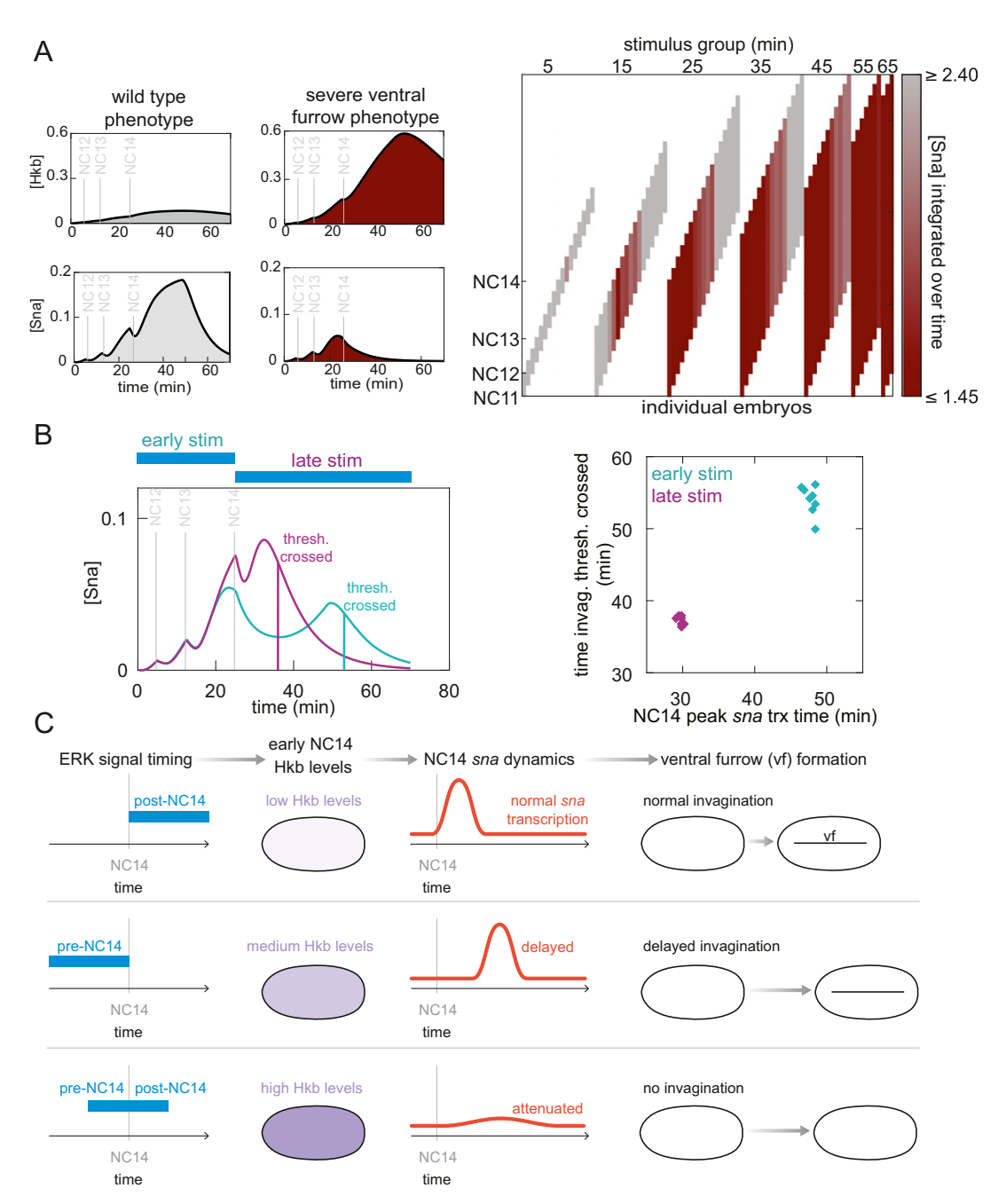


Fig. 4. A computational model of sna repression by Hkb recapitulates phenotypes and transcriptional dynamics induced by ectopic ERK signaling. (A) Model predictions for phenotypic severity, with Sna level in the ROI integrated over time used as a proxy for severity. On the left, trajectories of Hkb and Sna levels over time for two different stimulation conditions are shown. Low Sna (burgundy) over time results in severe phenotypes while high Sna (gray) results in low severity. High levels of Hkb correspond to low levels of Sna protein and vice versa. The plot on the right is comparable to Fig. 1C; each vertical bar represents an embryo and stimulation period; developmental time, counted in nuclear cycles, is on the y-axis; and embryos are grouped by stimulus duration, as indicated at the top of the plot. For integrated Sna levels between 1.45 and 2.40, colors scale from burgundy to gray. Embryos with an integrated Sna level ≥ 2.40 are color-coded gray to indicate wild-type phenotype, and embryos with an integrated Sna level ≤1.45 are color-coded burgundy to indicate the most severe phenotype. (B) Computational recreation of Fig. 2D accompanied by Sna dynamics in the ROI corresponding to early stimulation (turquoise) and late stimulation (plum). Blue bars indicate the stimulation period. Solid vertical lines indicate the time point at which the Sna trajectory indicated by the line's color exceeds the integrated Sna threshold required to initiate invagination (1.45). Each diamond on the righthand plot represents a different instance of the simulation (n = 20, 10 per condition). Stimulation condition is indicated by color. (C) A summary of this work: the timing of the ERK input translates to the timing (and presence) of ventral furrow formation via Hkb and sna. In the first column, the timing of ERK signals is shown by the positions of the blue bars relative to the onset of NC14. ERK signals are shown in order of increasing ability to suppress ventral furrow formation from top to bottom. ERK signals applied from the onset of NC14 onwards result in low Hkb levels during early NC14, indicated by the light color of the purple cartoon embryo. sna dynamics are similar to the wild type (orange curve labeled "normal sna transcription"), and ventral furrow formation occurs on a wild-type time scale, which is represented by the short arrow connecting the cartoons representing the pre- and postventral-furrow embryo. ERK signals applied prior to NC14 result in a moderate NC14 Hkb level (moderate purple), delayed NC14 sna transcription, and delayed ventral furrow invagination (longer arrow between pre- and postventral-furrow embryo). ERK signals applied prior to and directly after the onset of NC14 result in high NC14 Hkb levels (deep purple), attenuated NC14 sna transcription, and suppressed ventral furrows.

Downloaded at Princeton University Library on December 20, 2021

Our findings can also be interpreted in light of recent studies concerning Dl-based control of mesodermal cell fates. A recent optogenetic study identified early NC14 as a critical window for Dl induction of sna transcription and ventral furrow formation (48). The authors find that only a brief pulse of Dl signaling is needed in early NC14 to induce both sna and twi expression; then, later in NC14, sna expression is maintained by Twi. In contrast, the critical window during which ERK signaling is effective at repressing ventral furrow formation occurs slightly earlier, during NC13 and early NC14. This difference in timing is straightforward to rationalize: ERK must first trigger hkb expression so that Hkb is available to repress sna expression throughout the critical window for Dl activation. Our computational model also helps to explain why it is critical for *sna* expression to be induced in early NC14: because the number of sources of sna transcription doubles after each nuclear division cycle, NC14 is most effective for increasing Sna.

The secreted protein WntD is induced in cells exposed to both Dl and ERK signaling and is known to play a role in inhibiting Dl signaling at the posterior (21, 22, 24). Supporting this mode of regulation, we find that optogenetic ERK stimulation is able to potently induce wntD expression along the embryo's ventral surface as early as NC10 (Fig. 3C) and that embryos stimulated in this fashion exhibit a decrease in nuclear DI in late NC14 (SI Appendix, Fig. S10). Yet WntD appears to play a dispensable role in the decision to form a ventral furrow. This can be understood from a few observations. First, WntD appears to only exert an effect on Dl in late NC14, thus missing Dl's critical window in early NC14 for regulating sna expression. Second, comparing transcription from sna's proximal and distal enhancers reveals that Hkb, not WntD, is sufficient to explain ERK-induced transcriptional repression (Fig. 3D). We further show that genetic suppression of WntD activity through loss of its coreceptor Fz4 does not alter ERK's ability to suppress ventral furrow formation (SI Appendix, Fig. S4). Together, our data suggest that WntD's effects in the early embryo are restricted to other roles such as the shaping of the Dl gradient (23).

Our approach, combining optogenetic ERK stimulation with high-resolution transcriptional reporters and quantitative modeling, could be extended to study how signaling pathways work together to regulate additional features of the endoderm/mesoderm cell fate decision. Signaling-based control of cell movements and cell fates are related but not identical in the early Drosophila embryo. For example, in mesoderm determination, it is thought that sna is primarily responsible for cell movements, with twi being primarily responsible for cell fates (30). In endoderm differentiation, hkb and tll jointly regulate a network of transcription factors that establish multiple tissue types including hindgut, midgut, and visceral mesoderm (49). By varying the timing of the upstream ERK signal and following the dynamics of transcription factors far downstream, one could piece together the dynamic transcription profiles required for endodermal and mesoendodermal subpopulations or identify pathological signaling conditions that produce intermediate, unnatural fates.

More broadly, it remains to be seen how cells in other developmental contexts interpret time-varying, overlapping mesoendodermal cues. In the zebrafish embryo, for example, cells within 4 cell diameters of the blastoderm margin can give rise to either endodermal or mesodermal daughter cells and express markers for both fates (3, 5). The mesodermal marker *ntl* and the endodermal marker *gata5* are both expressed in response to signaling from the yolk cell, which activates *gata5* cell-autonomously and *ntl* through a relay mechanism that reaches cells further away (5). Endodermal cells go on to involute first, followed by mesodermal cells (6). It is likely that zebrafish endoderm- and mesoderm-related transcriptional dynamics are closely related to cell movement decisions, similar to what we have observed in the *Drosophila* embryo. An approach like the one we have taken here—dynamic interruption of signaling paired with monitoring of transcriptional dynamics and cell movement—could

shed light on how and when cell fate decisions are made across many model systems.

Materials and Methods

Drosophila Strains. UAS-optoSOS (19), P(mat α -GAL-VP16)mat67; P(mat α -GAL-VP16)mat15 (50), DI-Venus (27), MCP-mCherry (provided by Michael Levine's laboratory at Princeton University), sna BAC > MS2 (31), sna DE > MS2 (31), sna PE > MS2 (31), hkb > MS2 (26), wntD > MS2 (42), and y[1] w[67c23] fz4 [25-1] (Bloomington 38413) stocks were crossed (SI Appendix) to generate the stocks used in this study.

Microscopy. Either a patterned stripe or the entire field of view was illuminated using a Mightex Polygon digital micromirror device with an X-Cite XLED 450-nm blue light source. Live imaging was performed on a Nikon A1 RS confocal microscope with a 20× air objective (Princeton Microscopy Core). Embryos from UAS-optoSOS/P(matα-GAL-VP16)mat67; DI-Venus/P(matα-GAL-VP16)mat15 mothers were illuminated for 0.1 s every 20 s and imaged every 20 s at a single z-slice close to the embryo surface using a 514-nm laser. These stimulation conditions are comparable to those used in our previous work; 100 min of stimulation under this study's conditions induces the whole embryo squeeze induced by 60 min of stimulation under previous conditions (19). Embryos from UAS-optoSOS/P(matα-GAL-VP16)mat67; MCP-mCherry/P(matα-GAL-VP16)mat15 mothers and fathers containing an MS2 construct were illuminated for 0.1 s every 20 s and imaged every 20 s with a 561-nm laser, with z-stacks taken from the embryo surface to a depth of 8 μm with a step size of 0.5 μm.

Quantifying Ventral Furrow Invagination Delays. In wild-type embryos, the ventral furrow invaginates ~60 min after the onset of NC14. Invagination is synchronous. To calculate ventral furrow invagination delays in light-stimulated embryos, the time point at which nuclei first reappeared after the mitosis preceding NC14 was marked as the onset of NC14. Since invagination was often asynchronous in light-stimulated embryos, ventral furrow invagination was marked complete at the time point when the final region of the embryo anterior–posterior (AP) axis that one would expect to invaginate in a wild-type embryo invaginated. As time points were taken 20 s apart, the number of minutes between the onset of NC14 and completion of the ventral furrow was calculated by dividing the number of time points between the two events by 3.

Illumination Conditions for Studying the Effects of ERK Signal Timing on sna Transcriptional Dynamics. A ~60-min period of illumination was chosen for this experiment, as the time between the start of NC10 and the end of NC13 is ~60 min as is the time between the start of NC14 and the onset of ventral furrow invagination (51). For the early stimulation condition, illumination was initiated at the end of the mitosis preceding NC10 (when nuclei appear on the embryo surface) and maintained until the beginning of the mitosis following NC13. For the stimulation across the critical window, illumination was initiated at the beginning of the mitosis preceding NC12 and maintained for exactly 60 min. For the late stimulation, illumination was initiated at the beginning of the mitosis preceding NC14 and maintained for exactly 60 min.

Calculating % Region of Interest Invagination versus Mean Number of Active Nuclei in NC14. For each embryo, the number of transcribing nuclei was counted (SI Appendix) at each time point for the first 50 min of NC14 across the illuminated region (the region of interest, or ROI), a rectangle centered approximately around the most ventral medial point of the embryo extending ~200 μ m in the dorsoventral (DV) direction top-to-bottom and ~400 μ m in the AP position left-to-right. The number of transcribing nuclei was summed over all time points and divided by the number of time points (150, as images were taken every 20 s) to obtain the mean number of nuclei transcribing sna in NC14.

To calculate what fraction of the field of view invaginated, the field of view was partitioned into 30 μ m segments along the embryo AP axis. The numerator of the fraction consisted of the number of segments that invaginated within the first 260 min of developmental time (i.e., within the first ~150 min after the onset of NC14), and the denominator consisted of the total number of segments. In embryos in which posterior cell movement occurred, a position was considered to never have invaginated if posterior cell movement moved an AP segment out of the field of view before any invagination was witnessed. Because the field of view was never perfectly centered around the center of the embryo, some fields of view were placed more anterior or posterior than others, meaning that for a wild-type embryo, % ROI invagination could range from ~75% to 100%.

Calculating Time of Peak *sna* Transcription and Time of Invagination for Individual Segments along the Embryo AP Axis. Images of embryos were partitioned into $30~\mu m$ segments along the AP axis. We excluded any segments from our analysis

in which the height of the max-projected embryo in the DV direction was significantly smaller than the height of the embryo in the middle of the image to avoid undercounting the number of transcribing nuclei in the most terminal segments. The number of transcribing nuclei per embryo was recorded for each time point (every 20 s) in addition to the xy position where each transcription event occurred.

Active nuclei (i.e., nuclei transcribing sna) were identified at each time point and assigned to a segment according to their xy position (SI Appendix). Due to noise in the number of active nuclei per AP segment over time, time of peak sna transcription for each segment was identified from smoothed data: we summed the number of transcriptional events that occurred in the 5 min (15 time points) prior to and the 5 min after a given time point. The time point with the highest number of transcriptional events within this 10-min span was recorded as the time of peak sna transcription.

To connect the AP positions of invaginating segments to AP positions where the number of active nuclei had been counted, movies were rewound from the time of each segment's invagination to identify the original AP position of that segment. Time of invagination was counted from the onset of NC14, ~133 min developmental time (51). In cases in which ventral furrow invagination occurred after posterior cell movement had begun, the AP position of invagination for each segment was offset from the position at which transcribing nuclei had been counted.

Quantifying sna Enhancer Activity. To quantify the activity of the enhancer regions in the sna DE and sna PE MS2 constructs, we applied a stripe of blue light down the center of embryos from UAS-optoSOS/P(mat α -GAL-VP16)mat67; MCP-mCherry/P(mat α -GAL-VP16)mat15 mothers and fathers containing the MS2 construct. Embryos were positioned such that the AP axis lay horizontal along the field of view. The stripe covered the center 120 μ m of the AP axis, and the light was applied from NC10 to the end of NC14 using illumination conditions as detailed in *Microscopy*. The entire field of view (~480 μ m wide and 200 μ m tall) was imaged over the full illumination time course as detailed in *Microscopy*.

Images of embryos were partitioned into 30-µm segments along the AP axis, and transcribing nuclei were counted and assigned to segments (SI Appendix). For each embryo, the time point and segment with the highest number of transcribing nuclei were set as the denominator by which all other transcribing nuclei counts were divided. For each time point, all the values of the stimulated segments were averaged together, and all the values from unstimulated segments were averaged together. This resulted in two sna trajectories for each embryo: one for the stimulated region and one for the unstimulated region.

As the number of nuclei was small for each of the 30- μ m segments, the enhancer activity trajectories over time were noisy. Enhancer activity trajectories were smoothed using MATLAB's "smooth" function and a smoothing factor of 20 time points (400 s). The mean enhancer activity and enhancer activity SDs shown in Fig. 3D were calculated using the smoothed data.

Model Description. We used a mathematical model to describe the gene expression network proposed and refined in Fig. 3 A–D: ERK signaling induces expression of hkb, DI signaling induces expression of sna, and Hkb represses sna expression. As the ERK and DI signaling regimes are spatially distinct, we modeled their downstream interactions on the surface of a prolate spheroid that represents the surface of the embryo. Using a biophysical model from our previous work (44), we generated positions of nuclei on the surface of a prolate spheroid for NC11 through NC14 with statistical properties similar to a real embryo (SI Appendix, Fig. S5 A and B). Each nucleus in the embryo was represented by two spatial coordinates (θ , ϕ), and each cell was represented by a nucleus and the Voronoi cell that surrounds it (SI Appendix, Fig. S5 A and C).

ERK induces hkb expression by relieving Capicua (Cic) repression. We simulated the spatiotemporal profile of the fraction of Cic sites bound to DNA f (45) and the level of nuclear DI d (52) using previously existing models (SI Appendix, Fig. S5 D–G). We introduced a coupled model that includes a reaction–diffusion system and a gene regulatory network, in which in each cell i, each gene j is represented by two variables—the state of transcription (A_i^j) and the protein concentration (P_i^p). A_i^j stochastically flips between an on (1) and an off (0) state (Movie S3) in a manner that depends upon the rates of $k_{\text{on},i}^j$ and $k_{\text{off},i'}^j$ described below. Proteins diffuse through the cytoplasm and across cell membranes once membranes appear in NC14:

$$\frac{\partial P^j}{\partial t} = D^j \nabla^2 P^j + r^j.$$
 [1]

Using a finite volume approach, Eq. 1 was simplified to a set of ordinary

differential equations (ODEs) that describe the evolving levels of individual proteins in each cell (*SI Appendix*, Fig. S5C):

$$\frac{dP_i^j}{dt} = \sum_k \frac{\left(P_k^j - P_i^j\right) s_{ik}}{l_{ik}} + r_i^j,$$
 [2]

where k goes through all the neighbors of cell i, where s_{ik} is the length of Voronoi edge shared by cells i and k, and where l_{ik} is the distance between cells i and k. We assumed that translation was significantly faster than initiation of transcription, so a protein was synthesized in a cell only if it was transcriptionally active in that cell, but the protein degraded everywhere. Thus, r_i^i , the rate of production of protein j in cell i, was defined as:

$$r_i^j = A_i^j - k_{\text{deg}}^j P_i^j.$$
 [3]

The rate of initiating transcription $k_{\rm on}$ is a function of maternal signals and the levels of other proteins. We implemented the gene regulatory network through Eqs. 4 and 5 below. As we have only two genes in our network, sna and hkb, we replaced the index j with the gene names. Furthermore, since both sna and hkb expression attenuate toward the end of NC14, we set a time of attenuation $t_{\rm att}$ past which expression of hkb and sna become improbable:

$$k_{\text{on},i}^{\text{hkb}} = k_0^{\text{hkb}} (1 - f_i)^{m_1} \mathcal{H}(t - t_{\text{att}}),$$
 [4]

$$k_{\text{on},i}^{\text{sna}} = \frac{k_0^{\text{sna}}}{\left(1 + \left(d_i/d_0\right)^{-m_2}\right)\left(1 + \left(P_i^{\text{hkb}}/H_0\right)^{m_3}\right)} \mathcal{H}(t - t_{\text{att}}).$$
 [5]

If A_i^j is off (0) at time t, A_i^j switches to on at the next time point $t+\Delta t$ with probability $\exp(-k_{\text{on},i}^j(t)\Delta t)$. Conversely, if A_i^j is on (1), A_i^j switches to off at the next time point with probability $\exp(-k_{\text{off},i}^j(t)\Delta t)$. At the time of each mitosis, A_i^j is set to off for every gene and cell.

Estimating Phenotypic Severity from Protein Dynamics. We employed the integral of Sna protein (*F*) over time as a proxy for phenotypic severity, as *F* approximates the level of downstream factors seen across all nuclear cycles by the enhancer regions of the genes that more directly induce ventral furrow invagination:

$$F = \int_{T_{\text{init}}}^{T_{\text{end}}} \overline{P^{\text{Sna}}} dt,$$
 [6]

where $\overline{P^{\rm sna}}$ is the mean concentration of Sna in the region around the ventral furrow (*SI Appendix*, Fig. S5), $T_{\rm init}$ is the beginning of NC11, and $T_{\rm end}$ is 70 min into the simulation or 45 min into NC14. Due to the way the model was parameterized (44), developmental time moves more quickly in the model than in our experiments. Sixty minutes of experimental developmental time corresponds to 45 min of simulated developmental time.

We simulated F for stimulation conditions similar to those used in Fig. 1C using the best-fit parameter set (SI Appendix, Table S1). We used the observation that embryos averaging ~50 or more sna active nuclei exhibit wild-type ventral furrows (SI Appendix, Fig. S3) to set a mean Sna protein threshold level above which phenotypes of the simulated embryos were considered wild type. We plotted F as a function of active nuclei across nuclear cycles and found F_{max} , the threshold value that corresponds to 50 active nuclei, to be 2.4 (SI Appendix, Fig. S7). All simulated embryos with $F > F_{\text{max}}$ were colored gray in Fig. 4A to signify a wild-type phenotype. Conversely, embryos that average ~20 or fewer sna active nuclei across NC10 through NC14 exhibit the most severe phenotype (SI Appendix, Fig. S3). We found that 20 active nuclei corresponded to an F value of 1.45 (SI Appendix, Fig. S7), which we termed F_{min} . We set F_{min} as a second integrated Sna threshold value such that all embryos with $F < F_{\min}$ exhibited the most severe phenotype and were colored burgundy in Fig. 4A. All embryos with $F_{min} < F < F_{max}$ were assigned a phenotype severity color that scaled linearly from burgundy to gray according to the value of F.

Estimating Time of Invagination from Protein Dynamics. To estimate the time of ventral furrow formation, we noted the time T at which F crosses the threshold F_{\min} :

$$F = \int_{T_{\text{init}}}^{T} \overline{P^{\text{sna}}} dt = F_{\text{min}}.$$
 [7]

Data Availability. All study data are included in the article and/or supporting information.

figures, and the Flatiron Institute and the Lewis Sigler Institute for providing computing resources. This work was supported by the Hertz Fellowship and the NSF Graduate Research Fellowship Program (S.M.), NSF Faculty Early Career Development (CAREER) Award 1750663 (J.E.T.), and NIH Grant GM141843 (S.Y.S.).

- A. Grapin-Botton, D. Constam, Evolution of the mechanisms and molecular control of endoderm formation. Mech. Dev. 124, 253–278 (2007).
- S. Nowotschin, A.-K. Hadjantonakis, K. Campbell, The endoderm: A divergent cell lineage with many commonalities. *Development* 146, dev150920 (2019).
- A. Rodaway et al., Induction of the mesendoderm in the zebrafish germ ring by yolk cell-derived TGF-beta family signals and discrimination of mesoderm and endoderm by FGF. Development 126, 3067–3078 (1999).
- I. Burtscher, H. Lickert, Foxa2 regulates polarity and epithelialization in the endoderm germ layer of the mouse embryo. Development 136, 1029–1038 (2009).
- R. M. Warga, C. Nüsslein-Volhard, Origin and development of the zebrafish endoderm. Development 126, 827–838 (1999).
- R. M. Warga, C. B. Kimmel, Cell movements during epiboly and gastrulation in zebrafish. *Development* 108, 569–580 (1990).
- J. B. Skeath, The Drosophila EGF receptor controls the formation and specification of neuroblasts along the dorsal-ventral axis of the Drosophila embryo. *Development* 125, 3301–3312 (1998).
- Y. Yagi, T. Suzuki, S. Hayashi, Interaction between Drosophila EGF receptor and vnd determines three dorsoventral domains of the neuroectoderm. *Development* 125, 3625–3633 (1998).
- T. von Ohlen, C. Q. Doe, Convergence of dorsal, dpp, and egfr signaling pathways subdivides the drosophila neuroectoderm into three dorsal-ventral columns. *Dev. Biol.* 224, 362–372 (2000).
- M. Klingler, M. Erdélyi, J. Szabad, C. Nüsslein-Volhard, Function of torso in determining the terminal anlagen of the Drosophila embryo. Nature 335, 275–277 (1988).
- T. R. Strecker, S. R. Halsell, W. W. Fisher, H. D. Lipshitz, Reciprocal effects of hyper- and hypoactivity mutations in the Drosophila pattern gene torso. *Science* 243, 1062–1066 (1989).
- H. E. Johnson, J. E. Toettcher, Signaling dynamics control cell fate in the early Drosophila embryo. Dev. Cell 48, 361–370.e3 (2019).
- N. Perrimon, C. Pitsouli, B.-Z. Shilo, Signaling mechanisms controlling cell fate and embryonic patterning. Cold Spring Harb. Perspect. Biol. 4, a005975 (2012).
- R. E. Goldstein, G. Jiménez, O. Cook, D. Gur, Z. Paroush, Huckebein repressor activity in Drosophila terminal patterning is mediated by Groucho. *Development* 126, 3747–3755 (1999).
- R. Reuter, M. Leptin, Interacting functions of snail, twist and huckebein during the early development of germ layers in Drosophila. Development 120, 1137–1150 (1994).
- L. Dunipace, A. Ozdemir, A. Stathopoulos, Complex interactions between cisregulatory modules in native conformation are critical for Drosophila snail expression. *Development* 138, 4075–4084 (2011).
- Y. Kim et al., MAPK substrate competition integrates patterning signals in the Drosophila embryo. Curr. Biol. 20, 446–451 (2010).
- G. Brönner et al., Sp1/egr-like zinc-finger protein required for endoderm specification and germ-layer formation in Drosophila. Nature 369, 664–668 (1994).
- H. E. Johnson et al., The spatiotemporal limits of developmental Erk signaling. Dev. Cell 40, 185–192 (2017).
- A. L. Patel et al., Optimizing photoswitchable MEK. Proc. Natl. Acad. Sci. U.S.A. 116, 25756–25763 (2019).
- M. D. Gordon, M. S. Dionne, D. S. Schneider, R. Nusse, WntD is a feedback inhibitor of Dorsal/NF-kappaB in Drosophila development and immunity. *Nature* 437, 746–749 (2005).
- A. Helman et al., RTK signaling modulates the Dorsal gradient. Development 139, 3032–3039 (2012).
- N. Rahimi et al., A WntD-dependent integral feedback loop attenuates variability in Drosophila Toll signaling. Dev. Cell 36, 401–414 (2016).
- A. Ganguly, J. Jiang, Y. T. Ip, Drosophila WntD is a target and an inhibitor of the dorsal/twist/snail network in the gastrulating embryo. *Development* 132, 3419–3429 (2005).
- J. E. Toettcher, O. D. Weiner, W. A. Lim, Using optogenetics to interrogate the dynamic control of signal transmission by the Ras/Erk module. Cell 155, 1422–1434 (2013).
- H. E. Johnson, N. J. V. Djabrayan, S. Y. Shvartsman, J. E. Toettcher, Optogenetic rescue of a patterning mutant. Curr. Biol. 30, 3414–3424.e3 (2020).
- G. T. Reeves et al., Dorsal-ventral gene expression in the Drosophila embryo reflects the dynamics and precision of the dorsal nuclear gradient. Dev. Cell 22, 544–557 (2012).

- M. Coppey, A. N. Boettiger, A. M. Berezhkovskii, S. Y. Shvartsman, Nuclear trapping shapes the terminal gradient in the Drosophila embryo. Curr. Biol. 18, 915–919 (2008).
- Y. Goyal et al., Divergent effects of intrinsically active MEK variants on developmental Ras signaling. Nat. Genet. 49, 465–469 (2017).
- Y. T. Ip, K. Maggert, M. Levine, Uncoupling gastrulation and mesoderm differentiation in the Drosophila embryo. EMBO J. 13, 5826–5834 (1994).
- J. P. Bothma et al., Enhancer additivity and non-additivity are determined by enhancer strength in the Drosophila embryo. eLife 4, e07956 (2015).
- A. J. Manning, K. A. Peters, M. Peifer, S. L. Rogers, Regulation of epithelial morphogenesis by the G protein-coupled receptor mist and its ligand fog. Sci. Signal. 6, ra98 (2013).
- M. Costa, E. T. Wilson, E. Wieschaus, A putative cell signal encoded by the folded gastrulation gene coordinates cell shape changes during Drosophila gastrulation. *Cell* 76, 1075–1089 (1994).
- V. S. Chopra, M. Levine, Combinatorial patterning mechanisms in the Drosophila embryo. Brief. Funct. Genomics Proteomics 8, 243–249 (2009).
- K. Barrett, M. Leptin, J. Settleman, The Rho GTPase and a putative RhoGEF mediate a signaling pathway for the cell shape changes in Drosophila gastrulation. *Cell* 91, 905–915 (1997).
- U. Häcker, N. Perrimon, DRhoGEF2 encodes a member of the Dbl family of oncogenes and controls cell shape changes during gastrulation in Drosophila. Genes Dev. 12, 274–284 (1998).
- S. Etienne-Manneville, A. Hall, Rho GTPases in cell biology. Nature 420, 629–635 (2002).
- 38. A. B. Jaffe, A. Hall, Rho GTPases: Biochemistry and biology. *Annu. Rev. Cell Dev. Biol.* **21**, 247–269 (2005).
- V. Kölsch, T. Seher, G. J. Fernandez-Ballester, L. Serrano, M. Leptin, Control of Drosophila gastrulation by apical localization of adherens junctions and RhoGEF2. Science 315, 384–386 (2007).
- A. C. Martin, M. Kaschube, E. F. Wieschaus, Pulsed contractions of an actin-myosin network drive apical constriction. *Nature* 457, 495–499 (2009).
- A. C. Martin, M. Gelbart, R. Fernandez-Gonzalez, M. Kaschube, E. F. Wieschaus, Integration of contractile forces during tissue invagination. J. Cell Biol. 188, 735–749 (2010).
- 42. N. Rahimi *et al.*, Dynamics of Spaetzle morphogen shuttling in the *Drosophila* embryo shapes gastrulation patterning. *Development* **146**, dev181487 (2019).
- M. A. McElwain et al., A suppressor/enhancer screen in Drosophila reveals a role for wnt-mediated lipid metabolism in primordial germ cell migration. PLoS One 6, e26993 (2011).
- S. Dutta, N. J.-V. Djabrayan, S. Torquato, S. Y. Shvartsman, M. Krajnc, Self-similar dynamics of nuclear packing in the early Drosophila embryo. *Biophys. J.* 117, 743–750 (2019).
- S. Dutta, A. L. Patel, S. E. Keenan, S. Y. Shvartsman, From heterogeneous datasets to predictive models of embryonic development *bioRxiv* [Preprint] (2021). https://www. biorxiv.org/content/10.1101/2021.01.31.429006v1 (Accessed 9 February 2021).
- T. Schüpbach, E. Wieschaus, Maternal-effect mutations altering the anterior-posterior pattern of the Drosophila embryo. Rouxs Arch. Dev. Biol. 195, 302–317 (1986).
- D. Mitrossilis et al., Mechanotransductive cascade of Myo-II-dependent mesoderm and endoderm invaginations in embryo gastrulation. Nat. Commun. 8, 13883 (2017).
- J. Irizarry, J. McGehee, G. Kim, D. Stein, A. Stathopoulos, Twist-dependent ratchet functioning downstream from Dorsal revealed using a light-inducible degron. *Genes Dev.* 34, 965–972 (2020).
- J. A. Lengyel, D. D. Iwaki, It takes guts: The Drosophila hindgut as a model system for organogenesis. Dev. Biol. 243, 1–19 (2002).
- C. Hunter, E. Wieschaus, Regulated expression of nullo is required for the formation of distinct apical and basal adherens junctions in the Drosophila blastoderm. J. Cell Biol. 150, 391–401 (2000).
- V. E. Foe, G. M. Odell, B. A. Edgar, "Mitosis and morphogenesis in the Drosophila embryo: Point and counterpoint" in *The Development of Drosophila Melanogaster*, M. Bate, A. Martinez-Arias, Eds. (Cold Spring Harbor Laboratory Press, 1993), pp. 149–300.
- 52. J. S. Kanodia et al., Dynamics of the Dorsal morphogen gradient. *Proc. Natl. Acad. Sci. U.S.A.* **106**, 21707–21712 (2009).